01 Jan 2012

A Linear Energy Stable Scheme for a Thin Film Model Without Slope Selection

Wenbin Chen

Sidafa Conde

Cheng Wang

Xiaoming Wang
Missouri University of Science and Technology, xiaomingwang@mst.edu

et. al. For a complete list of authors, see https://scholarsmine.mst.edu/math_stat_facwork/1221

Recommended Citation

W. Chen et al., "A Linear Energy Stable Scheme for a Thin Film Model Without Slope Selection," *Journal of Scientific Computing*, vol. 52, no. 3, pp. 546 - 562, Springer, Jan 2012.
The definitive version is available at https://doi.org/10.1007/s10915-011-9559-2

J Sci Comput (2012) 52:546–562
DOI 10.1007/s10915-011-9559-2

A Linear Energy Stable Scheme for a Thin Film Model Without Slope Selection

Wenbin Chen · Sidafa Conde · Cheng Wang · Xiaoming Wang · Steven M. Wise

Received: 7 December 2010 / Revised: 2 November 2011 / Accepted: 8 November 2011 /
Published online: 26 November 2011

Abstract We present a linear numerical scheme for a model of epitaxial thin film growth without slope selection. The PDE, which is a nonlinear, fourth-order parabolic equation, is the L^2 gradient flow of the energy $\int_\Omega(-\frac{1}{2}\ln(1+|\nabla\phi|^2)+\frac{\epsilon^2}{2}|\Delta\phi(\mathbf{x})|^2)\,d\mathbf{x}$. The idea of convex-concave decomposition of the energy functional is applied, which results in a numerical scheme that is unconditionally energy stable, i.e., energy dissipative. The particular decomposition used here places the nonlinear term in the concave part of the energy, in contrast to a previous convexity splitting scheme. As a result, the numerical scheme is fully linear at each time step and unconditionally solvable. Collocation Fourier spectral differentiation is used in the spatial discretization, and the unconditional energy stability is established in the fully discrete setting using a detailed energy estimate. We present numerical simulation results for a sequence of ϵ values ranging from 0.02 to 0.1. In particular, the long time simulations show the $-\log(t)$ decay law for the energy and the $t^{1/2}$ growth law for the surface roughness, in agreement with theoretical analysis and experimental/numerical observations in earlier works.

Keywords Epitaxial thin film growth · Slope selection · Energy stability · Convexity splitting · Fourier collocation spectral

W. Chen
School of Mathematical Sciences, Fudan University, Shanghai 200433, China

S. Conde · C. Wang (✉)
Department of Mathematics, U. Massachusetts, Dartmouth, North Dartmouth, MA 02747-2300, USA
e-mail: cwang1@umassd.edu

X. Wang
Department of Mathematics, Florida State U., Tallahassee, FL 32306-4510, USA

S.M. Wise
Department of Mathematics, U. of Tennessee, Knoxville, TN 37996-1300, USA

1 Introduction

In this article we consider an efficient numerical scheme for a continuum $(2+1)$-dimensional model of epitaxial thin film growth. (See the review [2] for the recent history of such models of thin film growth.) The equation is the gradient flow associated with the following *energy* functional

$$E(\phi) := \int_\Omega \left(-\frac{1}{2}\ln(1+|\nabla\phi|^2) + \frac{\epsilon^2}{2}|\Delta\phi|^2 \right) \mathrm{d}\mathbf{x}, \tag{1}$$

where $\Omega = [0, L_x] \times [0, L_y]$, $\phi : \Omega \to \mathbb{R}$ is a periodic height function, and ϵ is a constant. We note that the first term, a non-quadratic term, represents the Ehrlich-Schwoebel effect, according to which adatoms (absorbed atoms) must overcome a higher energy barrier to stick to a step from an upper rather than from a lower terrace [1, 9, 10, 13]. This results in an uphill atom current in the dynamics and the steepening of mounds in the film. The second term, the quadratic term, represents the isotropic surface diffusion effect [10, 12]. We write

$$E^{ES}(\phi) := \int_\Omega F^{ES}(\nabla\phi)\,\mathrm{d}\mathbf{x}, \qquad F^{ES}(\mathbf{y}) := -\frac{1}{2}\ln(1+|\mathbf{y}|^2), \tag{2}$$

where $\mathbf{y} \in \mathbb{R}^2$ and $|\mathbf{y}| = \sqrt{y_1^2 + y_2^2}$. Hence, $E(\phi) = E^{ES}(\phi) + \frac{\epsilon^2}{2}\|\Delta\phi\|^2$ where $\|\cdot\|$ denotes the L^2 norm (rms).

The use of the Ehrlich-Schwoebel term (2) appears to have originated in the work [6]. Note that $F^{ES} : \mathbb{R}^2 \to \mathbb{R}$ is bounded above by 0 and unbounded below. In fact $F^{ES} \to -\infty$ as $|\mathbf{y}| \to \infty$. Furthermore, F^{ES} has no relative minima, which implies that there are no energetically favored values for $|\nabla\phi|$. Physically this means that there is no slope selection mechanism in the dynamics, at least from an energetic point of view, that could set a preferred slope of the height function ϕ. See the relevant discussions in [7, 8, 10, 11].

The chemical potential is defined to be the variational derivative of the energy (1), i.e.,

$$\mu := \delta_\phi E = \nabla \cdot \left(\frac{\nabla\phi}{1+|\nabla\phi|^2} \right) + \epsilon^2\Delta^2\phi. \tag{3}$$

Here we consider the gradient flow of the form

$$\partial_t\phi = -\mu = -\nabla \cdot \left(\frac{\nabla\phi}{1+|\nabla\phi|^2} \right) - \epsilon^2\Delta^2\phi, \tag{4}$$

where the boundary conditions for the height function ϕ are taken to be periodic in both spatial directions. We refer to (4) as the no-slope-selection equation, for reasons that will be apparent. Equation (4) may be rewritten in the form

$$\partial_t\phi = \nabla \cdot \left(\frac{|\nabla\phi|^2}{1+|\nabla\phi|^2}\nabla\phi \right) - \Delta\phi - \epsilon^2\Delta^2\phi. \tag{5}$$

In the small-slope regime, where $|\nabla\phi|^2 \ll 1$, (5) may be replaced by

$$\partial_t\phi = \nabla \cdot (|\nabla\phi|^2\nabla\phi) - \Delta\phi - \epsilon^2\Delta^2\phi, \tag{6}$$

which we refer to as the slope-selection equation [7, 8, 10, 12]. Solutions to (6), unlike those of (4), exhibit pyramidal structures, where the faces of the pyramids have slopes $|\nabla\phi| \approx 1$. Solutions to the no-slope-selection equation (4), on the other hand, exhibit mound-like structures, the slopes of which (on an infinite domain) may grow unbounded [10, 15]. Note that solutions of (6) and (4) have up-down symmetry, in an average sense. In other words, there is no way to distinguish a hill from a valley.

Typically one is interested in the how properties associated with the solutions to (4) and (6) scale with time, where ϵ is assumed small. The physically interesting quantities that may be obtained from the solutions of these equations are the surface roughness, defined as

$$w(t) = \sqrt{\frac{1}{|\Omega|}\int_\Omega \left|\phi(\mathbf{x},t) - \bar{\phi}(t)\right|^2 \mathrm{d}\mathbf{x}}, \quad \text{with } \bar{\phi}(t) = \frac{1}{|\Omega|}\int_\Omega \phi(\mathbf{x},t)\,\mathrm{d}\mathbf{x}, \tag{7}$$

the characteristic pyramid/mound size, denoted $\lambda(t)$, and the energy. For the slope-selection equation (6) numerical simulations and rigorous (as well as non-rigorous) scaling arguments have demonstrated that $w \sim O(t^{1/3})$, $\lambda(t) \sim O(t^{1/3})$, and $E \sim O(t^{-1/3})$. Likewise, for the no-slope-selection equation (4), one obtains $w \sim O(t^{1/2})$, $\lambda(t) \sim O(t^{1/4})$, and $E \sim O(-\ln(t))$. (See [10, 11] and references therein.) Observe that for the no-slope-selection equation (4), the average mound height (measured by the roughness) grows faster then the mound width (measured by λ), which is expected because there is no preferred slope of the height function ϕ. Also, note that in the rigorous setting, for example [7, 8, 11], one can only (at best) obtain lower bounds for the energy dissipation and, conversely, upper bounds for the roughness growth. However, the rates quoted as the upper or lower bounds are typically observed for the averaged values of the quantities of interest.

Practically speaking, predicting these scaling laws numerically is quite challenging, since they require very long simulation times. Moreover, these laws are expected to break down the closer one gets to the saturation time, which for the no-slope-selection equation (4) scales like $O(\epsilon^{-2})$. (See Figs. 2, 4, and 5 and the related discussion in Sect. 4. Also, see Fig. 1 of [11].) But the solution behavior is ill-understood, computationally and rigorously, near the saturation time. To adequately capture the full range of coarsening behaviors, numerical simulations for the coarsening process require short- and long-time accuracy and stability, in addition to high spatial accuracy for small values of ϵ. In this paper, we build on our previous work [15] by introducing an efficient linear, unconditionally stable, unconditionally solvable scheme for approximating solutions to the no-slope-selection equation (4). The scheme is based on a convexity splitting of the energy (1) into a purely convex part and a purely concave part.

The introduction of convexity splitting schemes is generally attributed to Eyre [3]. To numerically solve the Cahn-Hilliard and Allen-Cahn equations, Eyre proposed to decompose the Cahn-Hilliard energy, $E^{CH}(\phi) = \frac{1}{4}\|\phi\|_{L^4}^4 - \frac{1}{2}\|\phi\|_{L^2}^2 + \frac{\epsilon^2}{2}\|\nabla\phi\|_{L^2}^2$, into a convex part and a concave part. In the convexity splitting scheme, one treats the terms of the variational derivative implicitly or explicitly according to whether the terms correspond to the convex or concave parts of the energy, respectively. For the canonical decomposition of the Cahn-Hilliard energy above, one obtains the convexity splitting approximation

$$\mu^{k+1} = (\phi^{k+1})^3 - \phi^k - \epsilon^2\Delta\phi^{k+1}, \tag{8}$$

where, at the time continuous level, $\mu = \delta_\phi E^{CH}$ is the chemical potential relative to the energy. Eyre's convex-splitting scheme is first-order accurate in time, unconditionally uniquely solvable, and unconditionally energy stable in the sense that the energy is monotonically non-increasing in (discrete) time, regardless of the time step size. Such unconditionally stable schemes are highly desirable with regard to long time numerical simulation, especially for coarsening processes that require increasingly larger time step sizes for efficient computation.

We extended Eyre's convexity splitting idea in [15] to deal with terms in the chemical potential that are nonlinear in the gradients of ϕ. In particular, we applied the convexity

splitting methodology to develop schemes for both the slope-selection (6) and no-slope-selection (4) equations. In [15], our scheme for the latter equation was

$$\frac{\phi_1^{n+1}-\phi_1^n}{k}=-\mu^{k+1}=\nabla\cdot\left(\frac{\nabla\phi_1^{n+1}|\nabla\phi_1^{n+1}|^2}{1+|\nabla\phi_1^{n+1}|^2}\right)-\Delta\phi_1^n-\epsilon^2\Delta^2\phi_1^{n+1}. \tag{9}$$

This is based on the energy splitting

$$E(\phi)=\int_\Omega\left(\frac{1}{2}(|\nabla\phi|^2-\ln(1+|\nabla\phi|^2))+\frac{\epsilon^2}{2}|\Delta\phi(\mathbf{x})|^2\right)\mathrm{d}\mathbf{x}-\int_\Omega\frac{1}{2}|\nabla\phi|^2\,\mathrm{d}\mathbf{x}, \tag{10}$$

where it may be observed that the part associated with the first integral is convex, and the part associated with the second is concave. The primary drawback of the method (9) is that it is nonlinear. However, it may be observed that solving this scheme is equivalent to minimizing a strictly convex, coercive functional. This is a general feature of convexity splitting schemes [5, 14, 15]. In [15] we used a nonlinear conjugate gradient method to solve (9). This was a natural choice because of the convex nature of the problem at the implicit time level.

Other schemes have been developed for the no-slope-selection equation (4). (There are relatively more works devoted to the slope-selection equation (6). See, for example, [15, 16].) Li and Liu developed a spectral method in [10]. See also the computational results in [6]. However, besides our own work in [15], to our knowledge no one has analyzed any scheme for the no-slope-selection equation (4).

The main contribution of this manuscript is an alternate convex-concave decomposition of the energy (1) associated with the epitaxy thin film model without slope selection. It is observed that the nonlinear term $\ln(1+|\nabla\phi|^2)$ is bounded by $|\nabla\phi|^2$ in functional norms. Thus, instead of placing the nonlinear term in the convex part, we may—by appropriately adding and subtracting the term $\frac{1}{2}\|\nabla\phi\|^2$ in the energy—place the nonlinear part in the concave portion of the energy. As a result, the nonlinear term is treated *explicitly* in the convex splitting scheme; the scheme then becomes purely linear! More importantly, the linear operator involved in the scheme, which is positive and has constant coefficients, can be efficiently inverted by FFT or other existing fast linear solvers. This gives rise to a scheme that is vastly more efficient than the nonlinear counterpart (9) developed in [15]. In addition, this purely linear scheme also preserves the unconditional energy stability that was enjoyed by the nonlinear scheme, due to its convex splitting nature.

We will show that this energy dissipation property is valid for both the semi-discrete scheme (time discrete, space continuous) and the fully discrete scheme. In this paper, we use collocation Fourier spectral differentiation to effect spatial discretization. Another observation of the energy stability is that it can be derived by using an energy estimate other than the general convexity analysis we provided in [15]. Therefore, we could apply integration by parts in the collocation Fourier spectral differentiation and carry out the energy estimate at the discrete level. That in turn leads to unconditional stability with respect to the discrete energy.

The rest of the manuscript is organized as follows. In Sect. 2 we recall the energy stability result for general convex splitting schemes, present the alternate convex-concave decomposition of the energy (1), and formulate the corresponding purely linear numerical scheme. We show that the unconditional energy stability of the scheme may be derived by using either the general analysis from [15], or more directly using an energy estimate. In Sect. 3 we present the fully discrete scheme, where Fourier spectral differentiation is utilized in space. The energy stability will be established at the fully discrete level, based on integration by parts in Fourier space. In Sect. 4 we present some numerical simulation results. We offer our concluding remarks in Sect. 5.

2 The Numerical Scheme

2.1 Energy Stability of Convex Splitting Schemes

The natural function space for our problem is the subspace of $H^2(\Omega)$ whose functions are periodic and have zero average, which we denote by $\mathring{H}^2_{per}(\Omega)$. To begin, we consider a general energy functional of the form

$$E(\phi) = E^{ES}(\phi) + \frac{\epsilon^2}{2}\|\Delta\phi\|^2, \tag{11}$$

for all $\phi \in \mathring{H}^2_{per}(\Omega)$, where

$$E^{ES}(\phi) = \int_\Omega F^{ES}(\nabla\phi)\,\mathrm{d}\mathbf{x}, \tag{12}$$

and $F^{ES} : \mathbb{R}^2 \to \mathbb{R}$ is twice differentiable. We suppose that this F^{ES} can be decomposed (non-uniquely) into convex and concave terms—respectively, contractive and expansive terms in the language of Eyre [3]—in the sense that

$$F^{ES}(\mathbf{y}) = F^{ES}_c(\mathbf{y}) - F^{ES}_e(\mathbf{y}), \tag{13}$$

where $D^2_{\mathbf{y}}F^{ES}_c,\ D^2_{\mathbf{y}}F^{ES}_e \geq 0$. Subordinate to this decomposition of the energy density F we define the Ehrlich-Schwoebel-type energies

$$E^{ES}_c(\phi) := \int_\Omega F^{ES}_c(\nabla_{\mathbf{x}}\phi)\,\mathrm{d}\mathbf{x}, \qquad E^{ES}_e(\phi) := \int_\Omega F^{ES}_e(\nabla_{\mathbf{x}}\phi)\,\mathrm{d}\mathbf{x}, \tag{14}$$

so that $E^{ES}(\phi) = E^{ES}_c(\phi) - E^{ES}_e(\phi)$. The associated gradient flow is given by

$$\partial_t\phi = -\delta_\phi E^{ES}_c + \delta_\phi E^{ES}_e - \epsilon^2\Delta^2\phi, \tag{15}$$

where δ_ϕ is the variational derivative with respect to ϕ. The corresponding convex splitting numerical scheme for the gradient flow (15) with time step size $k > 0$ can be written as

$$\begin{aligned}\frac{\phi^{n+1}-\phi^n}{k} &= -\delta_\phi E^{ES}_c(\phi^{n+1}) + \delta_\phi E^{ES}_e(\phi^n) - \epsilon^2\Delta^2\phi^{n+1}\\ &= \nabla_{\mathbf{x}}\cdot\nabla_{\mathbf{y}}F^{ES}_c(\nabla_{\mathbf{x}}\phi^{n+1}) - \nabla_{\mathbf{x}}\cdot\nabla_{\mathbf{y}}F^{ES}_e(\nabla_{\mathbf{x}}\phi^n) - \epsilon^2\Delta^2\phi^{n+1}.\end{aligned} \tag{16}$$

Notice that this scheme in not uniquely defined, since the convex-concave splitting is not unique in general. This subtle fact will lead to the key observation of this article.

The following result guarantees the unconditional energy stability and convergence for the convex splitting scheme (16). Related results can also be found in [14].

Theorem 1 (Theorem 1 [15]) *Assume that the energy functional* (11) *is twice functional differentiable on* $\mathring{H}^2_{per}(\Omega)$, *and* $F^{ES}(\mathbf{y})$, $\nabla_{\mathbf{y}}F^{ES}(\mathbf{y})$ *grow at most polynomially in* $\mathbf{y}$. *Then the scheme given by* (16) *for the gradient system* (15) *satisfying the convexity splitting* (13) *is well-posed, with the solution given by the unique minimizer of the following modified energy functional*:

$$E_{scheme}(\phi) := \frac{\epsilon^2}{2}\|\Delta\phi\|^2 + E^{ES}_c(\phi) + \frac{1}{2k}\|\phi\|^2 - \int_\Omega\left(\delta_\phi E^{ES}_e(\phi^n) + \frac{1}{k}\phi^n\right)\phi\,\mathrm{d}\mathbf{x}. \tag{17}$$

Moreover, the energy is a non-increasing function of time, i.e., we have

$$E_{scheme}(\phi^{n+1}) \leq E_{scheme}(\phi^n) - \frac{1}{k}\|\phi^{n+1}-\phi^n\|^2 - \frac{\epsilon^2}{2}\|\Delta(\phi^{n+1}-\phi^n)\|^2, \quad \forall k > 0. \tag{18}$$

And, the solution to the scheme (16) *converges to the solution of the thin film epitaxy model* (15) *at vanishing time step size* ($k \to 0$) *on any finite time interval.*

As we have already mentioned, for the thin film model (4), we previously [15] proposed a convexity splitting of the form $E^{ES}(\phi) = E_c^{ES}(\phi) - E_e^{ES}(\phi)$, where

$$E_c^{ES}(\phi) = \int_\Omega \frac{1}{2}\{|\nabla\phi|^2 - \ln(1+|\nabla\phi|^2)\}\,d\mathbf{x}, \qquad E_e^{ES}(\phi) = \int_\Omega \frac{1}{2}|\nabla\phi|^2\,d\mathbf{x}. \tag{19}$$

The convex splitting scheme for the no-slope-selection equation (4) subordinate to this splitting is then given in (9). The energy stability of (9) is a corollary of Theorem 1.

2.2 A Linear Convex Splitting Scheme

The main contribution of this article is an alternate convexity splitting of the Ehrlich-Schwoebel energy E^{ES} for the thin film model without slope selection. Specifically, consider the splitting $E^{ES}(\phi) = E_c^{ES}(\phi) - E_e^{ES}(\phi)$, where

$$E_c^{ES}(\phi) = \int_\Omega \frac{1}{2}|\nabla\phi|^2\,d\mathbf{x}, \qquad E_e^{ES}(\phi) = \int_\Omega \frac{1}{2}\{|\nabla\phi|^2 + \ln(1+|\nabla\phi|^2)\}\,d\mathbf{x}. \tag{20}$$

The convexity of E_c^{ES} is obvious, and the convexity of E_e^{ES} comes from the convexity of the following function

$$G(\mathbf{y}) = \frac{1}{2}\{|\mathbf{y}|^2 + \ln(1+|\mathbf{y}|^2)\}. \tag{21}$$

The corresponding convex splitting numerical scheme is given by

$$\frac{\phi^{n+1}-\phi^n}{k} = \Delta\phi^{n+1} - \nabla\cdot\left(\frac{\nabla\phi^n}{1+|\nabla\phi^n|^2}\right) - \Delta\phi^n - \epsilon^2\Delta^2\phi^{n+1}. \tag{22}$$

Of course, the proposed scheme (22) is purely linear due to the explicit treatment of the nonlinear term. It can be reformulated as

$$\left(\frac{1}{k}I - \Delta + \epsilon^2\Delta^2\right)\phi^{n+1} = f^n := \frac{\phi^n}{k} - \nabla\cdot\left(\frac{\nabla\phi^n}{1+|\nabla\phi^n|^2}\right) - \Delta\phi^n. \tag{23}$$

Even without Theorem 1, it may observed that the scheme is unconditionally uniquely solvable. In fact, a simple calculation reveals that all the eigenvalues of the operator on the left hand side of (23) are positive. The main advantage of (22), over any other nonlinear scheme, is that spectral and fast elliptic solvers are directly applicable. This fact shows the importance of the alternate energy decomposition (20), where the nonlinear part of the energy can be transferred to the concave (expansive) part of the energy. And, according to the analysis in [14, 15], the concave part of the energy should always be treated explicitly in the numerical scheme.

2.3 Energy Stability via a Direct Proof

Because our linear scheme (22) is derived from a convexity splitting, namely, (20), the unconditional energy stability (18) and finite time convergence are guaranteed by Theorem 1. However, in the following we show the energy stability directly, without appealing to prior results.

Lemma 1 *Numerical solutions of* (22) *satisfy the energy dissipation inequality* (18). *In other words,* (22) *is an energy stable scheme.*

Proof Taking L^2 inner product of (22) with $\phi^{n+1}-\phi^n$ yields

$$-\frac{1}{k}\|\phi^{n+1}-\phi^n\|^2=\left(\phi^{n+1}-\phi^n,\nabla\cdot\left(\frac{\nabla\phi^n}{1+|\nabla\phi^n|^2}\right)\right)+(\phi^{n+1}-\phi^n,\Delta\phi^n)$$
$$-(\phi^{n+1}-\phi^n,\Delta\phi^{n+1})+\epsilon^2(\phi^{n+1}-\phi^n,\Delta^2\phi^{n+1}). \tag{24}$$

For the linear terms, integration by parts can be applied and the following equalities are standard:

$$(\phi^{n+1}-\phi^n,\Delta\phi^n-\Delta\phi^{n+1})=\|\nabla(\phi^{n+1}-\phi^n)\|^2, \tag{25}$$
$$(\phi^{n+1}-\phi^n,\Delta^2\phi^{n+1})=\frac{1}{2}\big(\|\Delta\phi^{n+1}\|^2-\|\Delta\phi^n\|^2\big)+\frac{1}{2}\|\Delta(\phi^{n+1}-\phi^n)\|^2. \tag{26}$$

For the nonlinear term, we also start with an integration by parts:

$$I:=\left(\phi^{n+1}-\phi^n,\nabla\cdot\left(\frac{\nabla\phi^n}{1+|\nabla\phi^n|^2}\right)\right)=-\left(\nabla\phi^{n+1}-\nabla\phi^n,\frac{\nabla\phi^n}{1+|\nabla\phi^n|^2}\right). \tag{27}$$

A careful calculation shows that

$$-\ln(1+|\nabla\phi^{n+1}|^2)+\ln(1+|\nabla\phi^n|^2)=\ln\left(\frac{1+|\nabla\phi^n|^2}{1+|\nabla\phi^{n+1}|^2}\right)$$
$$=\ln\left(1+\frac{|\nabla\phi^n|^2-|\nabla\phi^{n+1}|^2}{1+|\nabla\phi^{n+1}|^2}\right)$$
$$\le\frac{|\nabla\phi^n|^2-|\nabla\phi^{n+1}|^2}{1+|\nabla\phi^{n+1}|^2}, \tag{28}$$

where the last step follows from the inequality

$$\ln(1+r)\le r,\quad \forall r>-1. \tag{29}$$

Note that inequality (28) is a point-wise estimate, and it implies that

$$E^{ES}(\phi^{n+1})-E^{ES}(\phi^n)=\int_\Omega\left(-\frac{1}{2}\ln(1+|\nabla\phi^{n+1}|^2)+\frac{1}{2}\ln(1+|\nabla\phi^n|^2)\right)\mathrm{d}\mathbf{x}$$
$$\le\frac{1}{2}\int_\Omega\frac{|\nabla\phi^n|^2-|\nabla\phi^{n+1}|^2}{1+|\nabla\phi^{n+1}|^2}\,\mathrm{d}\mathbf{x}$$
$$=\int_\Omega\frac{-\frac{1}{2}(\nabla\phi^{n+1}+\nabla\phi^n)\cdot(\nabla\phi^{n+1}-\nabla\phi^n)}{1+|\nabla\phi^{n+1}|^2}\,\mathrm{d}\mathbf{x}. \tag{30}$$

The combination of (27) and (30) indicates that

$$I-\big[E^{ES}(\phi^{n+1})-E^{ES}(\phi^n)\big]$$
$$\ge\int_\Omega\left(\frac{-(\nabla\phi^{n+1}-\nabla\phi^n)\cdot\nabla\phi^n}{1+|\nabla\phi^n|^2}+\frac{\frac{1}{2}(\nabla\phi^{n+1}+\nabla\phi^n)\cdot(\nabla\phi^{n+1}-\nabla\phi^n)}{1+|\nabla\phi^{n+1}|^2}\right)\mathrm{d}\mathbf{x}. \tag{31}$$

Meanwhile, a careful calculation reveals the following point-wise estimate:

$$\frac{-(\nabla\phi^{n+1}-\nabla\phi^n)\cdot\nabla\phi^n}{1+|\nabla\phi^n|^2}+\frac{\frac{1}{2}(\nabla\phi^{n+1}+\nabla\phi^n)\cdot(\nabla\phi^{n+1}-\nabla\phi^n)}{1+|\nabla\phi^{n+1}|^2}$$
$$=\frac{-(\nabla\phi^{n+1}-\nabla\phi^n)\cdot\nabla\phi^n}{1+|\nabla\phi^n|^2}+\frac{(\nabla\phi^{n+1}-\nabla\phi^n)\cdot\nabla\phi^n}{1+|\nabla\phi^{n+1}|^2}$$

$$
\begin{aligned}
&- \frac{(\nabla\phi^{n+1} - \nabla\phi^n)\cdot\nabla\phi^n}{1+|\nabla\phi^{n+1}|^2} + \frac{\frac{1}{2}(\nabla\phi^{n+1} + \nabla\phi^n)\cdot(\nabla\phi^{n+1} - \nabla\phi^n)}{1+|\nabla\phi^{n+1}|^2} \\
&= -(\nabla\phi^{n+1} - \nabla\phi^n)\cdot\nabla\phi^n \cdot \frac{|\nabla\phi^{n+1}|^2 - |\nabla\phi^n|^2}{(1+|\nabla\phi^n|^2)(1+|\nabla\phi^{n+1}|^2)} + \frac{\frac{1}{2}|\nabla\phi^{n+1} - \nabla\phi^n|^2}{1+|\nabla\phi^{n+1}|^2} \\
&\geq -(\nabla\phi^{n+1} - \nabla\phi^n)\cdot\nabla\phi^n \cdot \frac{|\nabla\phi^{n+1}|^2 - |\nabla\phi^n|^2}{(1+|\nabla\phi^n|^2)(1+|\nabla\phi^{n+1}|^2)} \\
&= -(\nabla\phi^{n+1} - \nabla\phi^n)\cdot\nabla\phi^n \cdot \frac{(\nabla\phi^{n+1} + \nabla\phi^n)\cdot(\nabla\phi^{n+1} - \nabla\phi^n)}{(1+|\nabla\phi^n|^2)(1+|\nabla\phi^{n+1}|^2)} \\
&= -|\nabla\phi^{n+1} - \nabla\phi^n|^2 \cdot \frac{\nabla\phi^n\cdot(\nabla\phi^{n+1} + \nabla\phi^n)}{(1+|\nabla\phi^n|^2)(1+|\nabla\phi^{n+1}|^2)} \\
&\geq -|\nabla\phi^{n+1} - \nabla\phi^n|^2, \qquad (32)
\end{aligned}
$$

in which the last step comes from the fact that

$$
\begin{aligned}
\big(1+|\nabla\phi^n|^2\big)\big(1+|\nabla\phi^{n+1}|^2\big) &= 1 + |\nabla\phi^n|^2 + |\nabla\phi^{n+1}|^2 + |\nabla\phi^n|^2\cdot|\nabla\phi^{n+1}|^2 \\
&\geq |\nabla\phi^n|^2 + \nabla\phi^n\cdot\nabla\phi^{n+1}.
\end{aligned}
$$

Its substitution into (31) gives

$$
I - \big[E^{NS}(\phi^{n+1}) - E^{ES}(\phi^n)\big] \geq -\big\|\nabla(\phi^{n+1} - \phi^n)\big\|^2. \qquad (33)
$$

Finally, combining (24)–(26) and (33) results in

$$
\begin{aligned}
&E^{ES}(\phi^{n+1}) - E^{ES}(\phi^n) + \frac{\epsilon^2}{2}\big(\|\Delta\phi^{n+1}\|^2 - \|\Delta\phi^n\|^2\big) \\
&\leq -\frac{\epsilon^2}{2}\big\|\Delta(\phi^{n+1} - \phi^n)\big\|^2 - \frac{1}{k}\|\phi^{n+1} - \phi^n\|^2, \qquad (34)
\end{aligned}
$$

which is equivalent to (18) since $E(\phi) = E^{ES}(\phi) + \frac{\epsilon^2}{2}\|\Delta\phi\|^2$. □

3 Fully Discrete Linear Scheme

3.1 Definition and Unique Solvability

Since the boundary conditions are periodic and the differential operator in (23) is linear with constant coefficients, we use collocation Fourier spectral differentiation to effect spatial discretization. Assume that $L_x = N_x \cdot h_x$ and $L_y = N_y \cdot h_y$, for some mesh sizes h_x, $h_y > 0$ and some positive integers N_x and N_y. For simplicity of presentation, we use a square domain, i.e., $L_x = L_y = L$, and a uniform mesh size $h_x = h_y = h$, $N_x = N_y = N$ is taken. All the variables are evaluated at the regular numerical grid (x_i, y_j), with $x_i = ih$, $y_j = jh$, $0 \leq i,\ j \leq N$.

For a periodic function f over the given 2D numerical grid, assume its discrete Fourier expansion is given by

$$
f_{i,j} = \sum_{k,l=-[N/2]}^{[N/2]} \hat{f}_{k,l} \exp\left(\frac{2k\pi \mathrm{i} x_i}{L}\right) \exp\left(\frac{2l\pi \mathrm{i} y_j}{L}\right). \qquad (35)
$$

Then the Fourier spectral approximations to the first and second order partial derivatives are given by

$$(\mathcal{D}_{Nx} f)_{i,j} = \sum_{k,l=-[N/2]}^{[N/2]} \left(\frac{2k\pi \mathrm{i}}{L}\right) \hat{f}_{k,l} \exp\left(\frac{2k\pi \mathrm{i} x_i}{L}\right) \exp\left(\frac{2l\pi \mathrm{i} y_j}{L}\right), \tag{36}$$

$$(\mathcal{D}_{Ny} f)_{i,j} = \sum_{k,l=-[N/2]}^{[N/2]} \left(\frac{2l\pi \mathrm{i}}{L}\right) \hat{f}_{k,l} \exp\left(\frac{2l\pi \mathrm{i} x_i}{L}\right) \exp\left(\frac{2l\pi \mathrm{i} y_j}{L}\right), \tag{37}$$

$$(\mathcal{D}^2_{Nx} f)_{i,j} = \sum_{k,l=-[N/2]}^{[N/2]} \left(-\frac{4\pi^2 k^2}{L^2}\right) \hat{f}_{k,l} \exp\left(\frac{2k\pi \mathrm{i} x_i}{L}\right) \exp\left(\frac{2l\pi \mathrm{i} y_j}{L}\right), \tag{38}$$

$$(\mathcal{D}^2_{Ny} f)_{i,j} = \sum_{k,l=-[N/2]}^{[N/2]} \left(-\frac{4\pi^2 l^2}{L^2}\right) \hat{f}_{k,l} \exp\left(\frac{2k\pi \mathrm{i} x_i}{L}\right) \exp\left(\frac{2l\pi \mathrm{i} y_j}{L}\right). \tag{39}$$

The discrete Laplacian, gradient and divergence operators become

$$\begin{aligned} &\Delta_N f = \mathcal{D}^2_{Nx} f + \mathcal{D}^2_{Ny} f, \qquad \nabla_N f = \begin{pmatrix} \mathcal{D}_{Nx} f \\ \mathcal{D}_{Ny} f \end{pmatrix}, \\ &\nabla_N \cdot \begin{pmatrix} f_1 \\ f_2 \end{pmatrix} = \mathcal{D}_{Nx} f_1 + \mathcal{D}_{Ny} f_2, \end{aligned} \tag{40}$$

at the point-wise level. The fully discrete scheme is formulated as

$$\frac{\phi^{n+1} - \phi^n}{k} = -\nabla_N \cdot \left(\frac{\nabla_N \phi^n}{1 + |\nabla_N \phi^n|^2}\right) - \Delta_N \phi^n + \Delta_N \phi^{n+1} - \epsilon^2 \Delta_N^2 \phi^{n+1}. \tag{41}$$

It is straightforward to show that the fully discrete scheme (41) is unconditionally uniquely solvable. To see this consider a reformulation of (41) similar to (23):

$$\left(\frac{1}{k} I - \Delta_N + \epsilon^2 \Delta_N^2\right) \phi^{n+1} = f^n := \frac{\phi^n}{k} - \nabla_N \cdot \left(\frac{\nabla_N \phi^n}{1 + |\nabla_N \phi^n|^2}\right) - \Delta_N \phi^n. \tag{42}$$

Now, for each eigenfunction $\exp(\frac{2k\pi \mathrm{i} x_i}{L}) \exp(\frac{2l\pi \mathrm{i} y_j}{L})$, $-[\frac{N}{2}] \le k, l \le [\frac{N}{2}]$, the corresponding eigenvalue for the operator on the left hand side of (42) is precisely

$$\lambda_{k,l} := \frac{1}{k} - (\lambda_k + \lambda_l) + \epsilon^2 (\lambda_k + \lambda_l)^2, \tag{43}$$

where

$$\lambda_k = -\frac{4\pi^2 k^2}{L^2}, \qquad \lambda_l = -\frac{4\pi^2 l^2}{L^2}. \tag{44}$$

Consequently, $\lambda_{k,l} > 0$, which implies the unique unconditional solvability of the fully discrete scheme (41). Naturally, the FFT can be very efficiently utilized to obtain numerical solutions.

Remark 1 There are a couple of subtle details that we wish to point out. First, note that we are using collocation-type Fourier spectral differentiation, rather than Galerkin-type spectral differentiation. It is well-known that the discrete Fourier expansion (35) may contain aliasing errors, while the spectral accuracy is preserved as long as the exact solution is smooth enough. Also note that in the fully discrete scheme (41), the gradient is computed in Fourier space by using formulas (36)–(39), and the quotient of the terms $\nabla_N \phi$ and $1 + |\nabla_N \phi|^2$ in the nonlinear gradient term is then obtained in point-wise physical space. That greatly simplifies the computational effort required in the numerical simulations.

Our approach is very different from the Galerkin approach, wherein the nonlinear gradient term has to be expanded in all wave lengths. There is no simple formula to compute these coefficients, even if it is treated explicitly. In addition, in spite of aliasing errors appearing in the collocation spectral method, we are able to establish unconditional energy stability of the scheme at the fully discrete level, as we demonstrate in the next subsection.

3.2 Fully Discrete Energy Stability

Here we will define a fully discrete analogue of the energy (1) and will subsequently prove that a discrete version of the energy dissipation inequality (18) holds, regardless of the time step size k and independent of the spatial resolution N. To begin, given any periodic grid functions f and g (over the 2D numerical grid described above), the discrete approximations to the L^2 norm and inner product are given as

$$\|f\|_2 = \sqrt{\langle f, f\rangle}, \quad \text{with } \langle f, g\rangle = h^2 \sum_{i=0}^{N-1}\sum_{j=0}^{N-1} f_{i,j} g_{i,j}. \tag{45}$$

The discrete L^2 inner product can also be viewed in Fourier space with the help of a discrete version of Parseval's equality. In particular,

$$\langle f, g\rangle = L^2 \sum_{k,l=-[N/2]}^{[N/2]} \hat{f}_{k,l}\overline{\hat{g}_{k,l}} = L^2 \sum_{k,l=-[N/2]}^{[N/2]} \hat{g}_{k,l}\overline{\hat{f}_{k,l}}, \tag{46}$$

where $\hat{f}_{k,l}$, $\hat{g}_{k,l}$ are the Fourier coefficients of the grid functions f and g in expansions such as is given in (35). Detailed calculations show that the following discrete integration by parts formulae are valid:

$$\left\langle f, \nabla_N \cdot \begin{pmatrix} g_1 \\ g_2 \end{pmatrix} \right\rangle = -\left\langle \nabla_N f, \begin{pmatrix} g_1 \\ g_2 \end{pmatrix} \right\rangle, \tag{47}$$

$$\langle f, \Delta_N g\rangle = -\langle \nabla_N f, \nabla_N g\rangle, \qquad \langle f, \Delta_N^2 g\rangle = \langle \Delta_N f, \Delta_N g\rangle. \tag{48}$$

We now define the fully discrete energy via

$$\begin{aligned} E_N(\phi) &= E_N^{ES}(\phi) + \frac{\epsilon^2}{2}\|\Delta_N \phi\|_2^2, \\ E_N^{ES}(\phi) &= h^2 \sum_{i=0}^{N-1}\sum_{j=0}^{N-1}\left(-\frac{1}{2}\ln(1 + |\nabla_N \phi|^2)_{i,j}\right). \end{aligned} \tag{49}$$

The following proposition is the main theoretical result for the fully discrete scheme (41).

Proposition 1 *Numerical solutions of the scheme* (41) *satisfy*

$$E_N(\phi^{n+1}) \le E_N(\phi^n) - \frac{1}{k}\|\phi^{n+1} - \phi^n\|_2^2 - \frac{\epsilon^2}{2}\left\|\Delta_N(\phi^{n+1} - \phi^n)\right\|_2^2, \quad \forall k > 0. \tag{50}$$

In other words, (41) *is a discrete-energy stable scheme*.

Proof All of the calculations and estimates in (24)–(34) can be extended for the fully discrete scheme (41), with the discrete operators defined in (40) replacing their continuous counter parts, and the formulae in (47) and (48) replacing integration by parts. In particular,

note that the point-wise estimates (28) and (32) remain valid in the fully discrete case. As a result, one obtains

$$E_N^{ES}(\phi^{n+1}) - E_N^{ES}(\phi^n) + \frac{\epsilon^2}{2}\big(\|\Delta_N\phi^{n+1}\|_2^2 - \|\Delta_N\phi^n\|_2^2\big)$$
$$\leq -\frac{\epsilon^2}{2}\big\|\Delta_N(\phi^{n+1}-\phi^n)\big\|_2^2 - \frac{1}{k}\|\phi^{n+1}-\phi^n\|_2^2, \tag{51}$$

which is equivalent to (50). □

Remark 2 We point out that the unconditional energy stability of the fully discrete scheme can also be verified using a convexity argument, just as in the space-continuous case. For the pure Galerkin approximation, the only major modification needed is to view the "energy" as defined on the finite dimensional Galerkin space, compute the variational derivatives within the same Galerkin projected space, and view the fully discrete scheme as time discretization of a gradient flow on the finite dimensional Galerkin projected space.

For collocation spectral approach we have taken in (41), the convexity argument still works with the discrete derivatives and norms defined as above, and the integral is replaced by a finite sum, just as in the definition of the discrete inner product in the physical space.

4 Numerical Simulation Results

Now we show some numerical simulation results using the proposed linear splitting scheme (41) for the no-slope-selection equation (4), with a sequence of physical parameters $\epsilon = 0.1 : -0.01 : 0.02$. For the domain we take $L = L_x = L_y = 12.8$ and $h = L/N$, where h is the uniform spatial step size. Our numerical experiments have shown that the resolution $N = 384$ for $\epsilon = 0.1 : -0.01 : 0.05$ and $N = 512$ for $\epsilon = 0.04 : -0.01 : 0.02$ is adequate to resolve the small structures in the solution. (See the discussion below.) For the temporal step size k, we use $k = 0.001$ on the time interval $[0, 400]$, $k = 0.01$ on the time interval $[400, 6000]$, $k = 0.04$ on the time interval $[6000, 10^5]$ and $k = 0.08$ for $t > 10^5$ if needed. Figure 1 presents time snapshots of the film height ϕ with $\epsilon = 0.02$. Significant coarsening in the system is evident. At early times many small hills (red) and valleys (blue) are present. At the final time, $t = 300000$, a one-hill-one-valley structure emerges, and further coarsening is not possible.

The long time characteristics of the solution, especially the energy decay rate and surface roughness growth rate, are of interest to physicists and engineers. Recall that, at the space-discrete level, the energy is defined via (49). The space-continuous surface roughness is defined in (7), and an analogous fully discrete version is also available. At the PDE level, the lower bound for the energy decay rate is of the order of $-\ln(t)$, and the upper bound for the standard deviation growth rate is of the order of $t^{1/2}$, as established for the no-slope-selection equation (4) in Li and Liu's work [11]. Our numerical simulation results support these bounds. Figures 2 and 3 present the semi-log plots for the energy versus time and log-log plots for the roughness versus time, respectively, with the chosen sequence of physical parameters $\epsilon = 0.02 : 0.01 : 0.1$. The detailed scaling "exponents" obtained using least squares fits of the computed data up to time $t = 400$ are provided in Table 1. A clear observation of the $-\ln(t)$ and $t^{1/2}$ scaling laws can be made, with different coefficients dependent upon ϵ.

To confirm the robustness of the simulation results, we performed some numerical experiments testing the sensitivity of the computations to the initial random data and the numerical

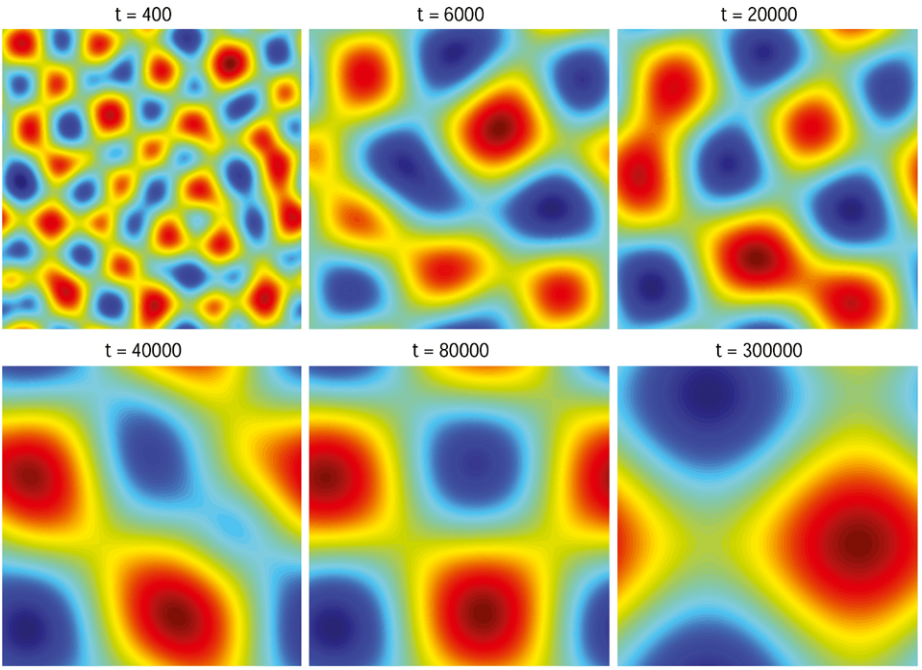

Fig. 1 (Color online) Snapshots of the computed height function ϕ at the indicated times for the parameters $L = 12.8$, $\epsilon = 0.02$. Note that the *color scale* changes with time. The hills (*red*) at early times are not as high as time at later times, and similarly with the valley (*blue*). To see how the average height/depth changes with time, see Fig. 3

Table 1 Fitting parameters for the least squares lines in Figs. 2 and 3. Specifically, the energy decay lines in Fig. 2 have the form $m_e \ln(t) + b_e$, and the roughness lines in Fig. 3 have the form $b_r t^{m_r}$. Least squares fits were computed using the physical data up to time $t = 400$. This was to avoid the later-time effects associated to the periodic boundary conditions

ϵ	0.02	0.03	0.04	0.05	0.06	0.07	0.08	0.09	0.10
m_e	−39.62	−38.84	−39.39	−38.21	−38.02	−38.67	−38.66	−39.80	−37.37
b_e	−154.24	−125.17	−98.50	−83.66	−74.27	−58.72	−47.06	−37.70	−36.67
m_r	0.52	0.52	0.51	0.52	0.55	0.55	0.55	0.57	0.56
b_r	0.38	0.38	0.37	0.36	0.34	0.34	0.33	0.32	0.31

resolution. For instance, using the parameter $\epsilon = 0.02$, a simulation with the higher spatial resolution $N = 768$ and the smaller time step $k = 0.000625$ was undertaken up to $t = 400$. Qualitative and quantitative comparisons between the base-line and high-level resolutions confirmed that the energy dissipation and surface roughness growth rates were nearly identical.

Now we recall that a lower bound for the energy (1), assuming $\Omega = (0, L) \times (0, L)$, has been derived in our earlier article [15]. In particular, based on the following estimate

$$F(\mathbf{y}) = -\frac{1}{2}\ln\bigl(1 + |\mathbf{y}|^2\bigr) \geq -\frac{1}{2}\bigl(\alpha|\mathbf{y}|^2 - \ln(\alpha) + \alpha - 1\bigr), \quad \forall \alpha \leq 1, \tag{52}$$

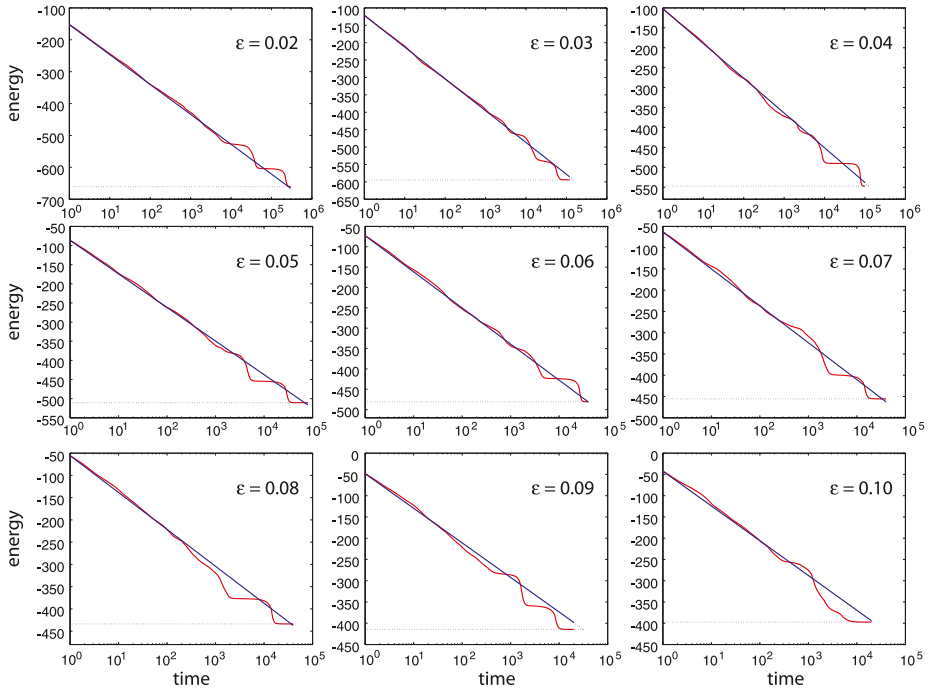

Fig. 2 (Color online) Semi-log plots of the temporal evolution the energy, for a sequence of ϵ values. The energy decreases like $-\ln(t)$ until saturation. The *dotted lines* correspond to the minimum energy reached by the numerical simulation. The *red lines* represent the energy plot obtained by the simulations, while the *straight lines* are obtained by least squares approximations to the energy data. The least squares fit is only taken for the linear part of the calculated data, only up to about time $t = 400$. Parameters for the fitted lines, which have the form $m_e \ln(t) + b_e$, can be found in Table 1

and the elliptic regularity estimate in 2-D

$$\|\Delta\phi\|^2 \geq 4\frac{\pi^2}{L^2}\|\nabla\phi\|^2, \quad \forall\phi \in H^2_{per}(\Omega), \tag{53}$$

with the choice of $\alpha = \frac{4\epsilon^2\pi^2}{L^2}$, we obtain a lower bound for the energy of the form[1]

$$E(\phi) \geq \frac{L^2}{2}\left(\ln\left(\frac{4\epsilon^2\pi^2}{L^2}\right) - \frac{4\epsilon^2\pi^2}{L^2} + 1\right) =: \gamma. \tag{54}$$

Obviously, since the energy is bounded below it cannot keep decreasing at the rate $-\ln(t)$. This fact manifests itself in the calculated data as the rate of decrease of the energy, for example, begins to wildly deviate from the predicted $-\ln(t)$ curve. Sometimes the rate of decrease increases, and sometimes it slows as the systems "feels" the periodic boundary conditions. Interestedly, regardless of this later-time deviation from the accepted rates, the time at which the system saturates (i.e., the time when the energy abruptly and essentially stops decreasing) is roughly that predicted by extending the blue lines in Fig. 2 to the predicted minimum energy (54). See the discussion below. As can be seen from the results

[1] We have here corrected a slight error in the bound presented in [15].

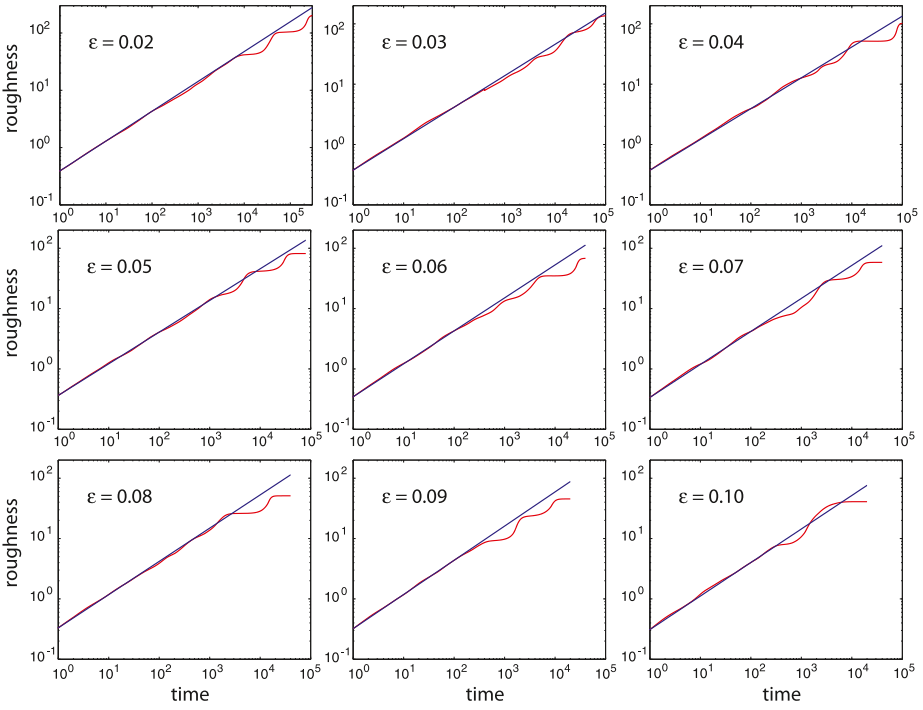

Fig. 3 (Color online) The log-log plot of the standard deviation (or roughness) of ϕ, denoted $w(t)$, for a sequence of ϵ values. For the no slope selection model, $w(t)$ grows like $t^{1/2}$. The *red lines* represent the plot obtained by the numerical simulations, while the *straight lines* are linear least squares approximations to the $t^{1/2}$ growth. The least squares fit is only taken for the linear part of the calculated data, only up to about time $t = 400$. In particular, the parameters for the (*blue*) fitting lines, which have the form $b_r t^{m_r}$, can be found in Table 1

of the numerical simulations, although such a bound is not sharp, the calculated minimum energies for different ϵ match those predicted by the formula to within 3% accuracy. See Fig. 4.

The dependence of the saturation time on the physical parameter ϵ can be formally predicted using the technique described above (i.e., by extending the $-\ln(t)$ line to the minimum energy γ). This type of formal argument suggests an intuitive $O(\epsilon^{-2})$ law for the saturation time scale, owing to the specific dependence of γ on ϵ. We now explore this saturation time dependence in our numerical simulation results. For each ϵ, the corresponding energy plot indicates an approximate $-\ln(t)$ law, with appropriate coefficients given in Table 1. We define the numerical saturation time as that time when the blue line in Fig. 2 meets the lowest calculated energy for the simulation. This lowest energy is reported in Fig. 4 for each value of ϵ. The deviation from γ is only about 3%. This lowest energy always corresponded to a state that features a one-up-one down hill and valley configuration, as in Fig. 1 for $t = 300000$.

Figure 5 gives the plot of the numerical saturation time versus ϵ. The star lines represent the values obtained by the numerical simulations, while the circle lines give the least square approximation to these numerical data. This approximation gives a slope of -2.04, which is almost a perfect match with the $O(\epsilon^{-2})$ scaling law. We note that not many works have

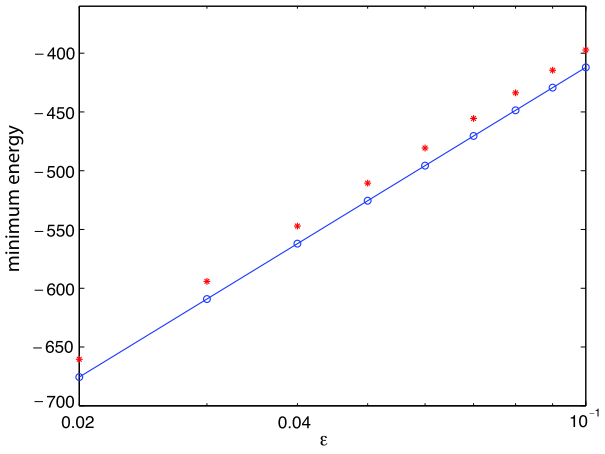

Fig. 4 (Color online) Minimum energy versus ϵ. The *star points* represent the calculated minimum energy at saturation. The *circles* indicate values of the energy lower bound from (54)

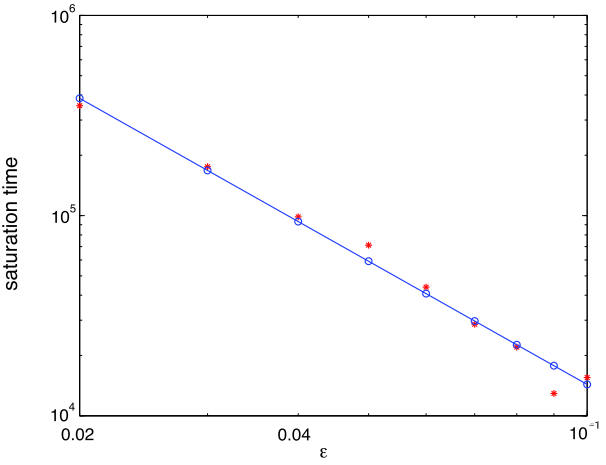

Fig. 5 Log-log plot of saturation time versus ϵ. The *star points* represent the values obtained by the numerical simulation, and the *line with circles* represent the least squares approximation to these data. The slope of the fitting line is -2.04

explored the saturation, in part, we believe, because these data are costly to obtain. As we have pointed out, convexity splitting schemes are well suited to these types of calculations, because of their unconditional stability properties.

5 Summary and Remarks

We have presented an unconditionally stable, unconditionally solvable, and convergent linear scheme for a model for thin film epitaxy without slope selection, i.e., the non-slope-selection equation (4). The unconditional stability and solvability and the convergence follow directly from our theory on convex splitting schemes for a certain class of epitaxial growth models [15]. The current scheme is fully linear in the sense that only a linear symmetric (bi-harmonic type) problem is solved at each time step. The unconditional stability and solvability of the fully discrete scheme derived using collocation-type Fourier spectral differentiation was also demonstrated. The new scheme was then implemented utilizing FFT. The physical scaling laws relevant for this model, in particular, the energy decay rate, the surface roughness growth rate, and saturation time were recovered and verified numerically.

The work here demonstrates an important subtlety regarding the non-uniqueness of the convex splitting method. In particular, although all of the (true) convexity splitting scheme enjoy unconditional stability, some splitting choices can be much more advantageous than others. Here by a different choice of splitting we obtained a linear scheme, that is much more efficient than the nonlinear scheme we proposed earlier [15].

We should point out that the technique applied here is not completely general. In other words, it is not always possible to derive a linear convex splitting scheme for genetic energy functionals. For example, one cannot derive a linear convex splitting scheme for gradient flows involving the standard quartic energy density $g(u) = \frac{1}{4}u^4 - \frac{1}{2}u^2$, because there is no splitting parameter $A > 0$ that guarantees $g_e(u) := \frac{A}{2}u^2 - \frac{1}{4}u^4$ is globally convex. On the other hand, the technique will find greater applicability than the specific model considered here. To see this, consider the point-wise, double-well energy density $g(u) = \frac{1}{2}u^2 - \ln(1 + x^2)$, which has relative minima at $u = \pm 1$. This has the convex splitting $g = g_c - g_e$, where $g_c(u) = (\frac{1}{2} + A)u^2$ and $g_e(u) = (Au^2 + \ln(1 + x^2))$. The last term is convex if $A \geq \frac{1}{8}$. Of course, here we are taking advantage of the fact that polynomials will dominate logarithms for large numbers, as we did in the present thin film context (cf. the discussion before (21)).

Furthermore, this technique can be used to handle nonlocal terms in the energy, such as those that come into play in the nonlocal Cahn-Hilliard equation [4]. For instance, consider the nonlocal energy

$$G(u) = \frac{1}{4}\int_\Omega \int_\Omega J(\mathbf{x} - \mathbf{y})\big(u(\mathbf{x}) - u(\mathbf{y})\big)^2 \,\mathrm{d}\mathbf{y}\,\mathrm{d}\mathbf{x},$$

where J is even, positive, and periodic on the rectangular domain Ω, and $u \in L^2(\Omega)$. This energy is already convex. Taking $G_c \equiv G$ and $G_e \equiv 0$ one obtains a linear—though nonlocal—convolution operator in the implicit part of the chemical potential. It is possible to avoid this situation by pushing the convolution to the explicit term, rather than the implicit. Specifically, it is straightforward to show that there is a convex splitting $G = G_c - G_e$ of the form [4]

$$\begin{aligned} G_c(u) &= \|J\|_1\|u\|_2^2, \\ G_e(u) &= \|J\|_1\|u\|_2^2 - \frac{1}{4}\int_\Omega \int_\Omega J(\mathbf{x} - \mathbf{y})(u(\mathbf{x}) - u(\mathbf{y}))^2 \,\mathrm{d}\mathbf{y}\,\mathrm{d}\mathbf{x}. \end{aligned}$$

Here the convolution goes to the explicit part of the chemical potential and therefore does not need to be inverted.

Acknowledgements The work is supported in part by the National Science Foundation, specifically, DMS-0606671, DMS-1008852, DMS-1002618 (X. Wang), DMS-0818030, DMS-1115390 (S.M. Wise), DMS-0802974 (S. Conde), and DCNS-0959382, DMS-1115420 (C. Wang), the Ministry of Education of China and the State Administration of Foreign Experts Affairs of China under 111 project grant B08018 (W. Chen), and the Natural Science Foundation of China 11171077 (W. Chen).

References

1. Ehrlich, G., Hudda, F.G.: Atomic view of surface diffusion: tungsten on tungsten. J. Chem. Phys. **44**, 1036–1099 (1966)
2. Evans, J.W., Thiel, P.A., Bartelt, M.C.: Morphological evolution during epitaxial thin film growth: formation of 2D islands and 3D mounds. Surf. Sci. Rep. **61**, 1–128 (2006)
3. Eyre, D.J.: Unconditionally gradient stable time marching the Cahn-Hilliard equation. In: Bullard, J.W., Kalia, R., Stoneham, M., Chen, L.Q. (eds.) Computational and Mathematical Models of Microstructural Evolution, vol. 53, pp. 1686–1712. Materials Research Society, Warrendale (1998)

4. Guan, Z., Wang, C., Wise, S.M.: Convergence of a convex splitting scheme for the nonlocal Cahn-Hilliard Equation (in preparation)
5. Hu, Z., Wise, S.M., Wang, C., Lowengrub, J.S.: Stable and efficient finite-difference nonlinear-multigrid schemes for the Phase Field Crystal equation. J. Comput. Phys. **228**, 5323–5339 (2009)
6. Johnson, M.D., Orme, C., Hunt, A.W., Graff, D., Sudijono, J., Sander, L.M., Orr, B.G.: Stable and unstable growth in molecular beam epitaxy. Phys. Rev. Lett. **72**, 116–119 (1994)
7. Kohn, R.V.: Energy-driven pattern formation. In: Sanz-Solé, M., Soria, J., Varona, J.L., Verdera, J. (eds.) Proceedings of the International Congress of Mathematicians, vol. 1, pp. 359–383. European Mathematical Society Publishing House, Madrid (2006)
8. Kohn, R.V., Yan, X.: Upper bound on the coarsening rate for an epitaxial growth model. Commun. Pure Appl. Math. **56**, 1549–1564 (2003)
9. Li, B.: High-order surface relaxation versus the Ehrlich-Schwoebel effect. Nonlinearity **19**, 2581–2603 (2006)
10. Li, B., Liu, J.-G.: Thin film epitaxy with or without slope selection, EURO. J. Appl. Math. **14**, 713–743 (2003)
11. Li, B., Liu, J.-G.: Epitaxial growth without slope selection: energetics, coarsening, and dynamic scaling. J. Nonlinear Sci. **14**, 429–451 (2004)
12. Moldovan, D., Golubovic, L.: Interfacial coarsening dynamics in epitaxial growth with slope selection. Phys. Rev. E **61**, 6190–6214 (2000)
13. Schwoebel, R.L.: Step motion on crystal surfaces: II. J. Appl. Phys. **40**, 614–618 (1969)
14. Wise, S.M., Wang, C., Lowengrub, J.: An energy stable and convergent finite-difference scheme for the Phase Field Crystal equation. SIAM J. Numer. Anal. **47**, 2269–2288 (2009)
15. Wang, C., Wang, X., Wise, S.M.: Unconditionally stable schemes for equations of thin film epitaxy. Discrete Contin. Dyn. Syst., Ser. A **28**, 405–423 (2010)
16. Xu, C., Tang, T.: Stability analysis of large time-stepping methods for epitaxial growth models. SIAM J. Numer. Anal. **44**, 1759–1779 (2006)